Zintl-phase compounds with $SnSb_4$ tetrahedral anions: Electronic structure and thermoelectric properties

Lijun Zhang, Mao-Hua Du, and D. J. Singh
Materials Science and Technology Division, Oak Ridge National Laboratory, Oak Ridge, Tennessee 37831-6114, USA
(Received 13 November 2009; revised manuscript received 23 January 2010; published 22 February 2010)

We report the investigation of Zintl-phase $Na(K)_8SnSb_4$ and related compounds that contain $SnSb_4$ tetrahedral anions using first principles electronic structure, Boltzmann transport, and density functional phonon calculations. We find that these compounds are narrow-gap semiconductors and there is a combination of heavy and light bands at valence band edge, which may lead to a combination of high thermopower and reasonable conductivity. High values of the thermopower are found for *p*-type doping within the Boltzmann transport theory. Furthermore, these materials are expected to have low thermal conductivity due to their structures that consist of a network of weakly coupled $SnSb_4$ clusters, which leads to low phonon frequencies. In particular, we find low-frequency optical phonons that should effectively scatter the heat-carrying acoustic phonons. These results are discussed in terms of the structure, which consists of anionic clusters. Based on the results, it is suggested that such compounds may represent a useful paradigm for finding new thermoelectric materials.

DOI: 10.1103/PhysRevB.81.075117 PACS number(s): 72.15.Jf, 71.20.Lp

I. INTRODUCTION

Waste heat recovery through thermoelectric generators is a promising way to alleviate the pressure from increasing demand for energy and global warming from CO_2 emission. However, the performance of commonly used thermoelectric materials is only $\sim 10\%$ of the thermodynamic limit, $\eta_c = \Delta T/T_h$ ($\Delta T = T_h - T_c$, where T_h and T_c are the temperatures of the hot and cold sides of a device, respectively). This and the related need for better thermoelectric cooling devices has motivated considerable recent effort to find new higher performance thermoelectric materials.[1–3]

The primary materials parameter governing the maximum efficiency of a thermoelectric device is the dimensionless figure of merit, $ZT = \sigma S^2 T/(\kappa_e + \kappa_l)$, where σ is the electrical conductivity, S is the Seebeck coefficient (thermopower), κ_e and κ_l are the electronic and lattice thermal conductivity, and T is temperature. High ZT requires high thermopower,[4] and a suitable combination of good carrier mobility, and low thermal conductivity. High thermopower is usually found in semiconductors with heavy band mass. High carrier mobility, on the other hand, needs small carrier effective mass and small electron-phonon and defect scattering. The lattice thermal conductivity and the thermopower play particularly important roles in this formula. This is because the electrical conductivity and the electronic part of the thermal conductivity are generally connected by the Wiedemann Franz relation.[4]

In principle, materials with large dielectric constants can better screen charged impurities or defects and thus reduce carrier scattering. Narrow-gap semiconductors often have high dielectric constants and are usually readily doped both *n* and *p* types. Transport within metals and degenerately doped semiconductors (including thermoelectrics) is often discussed using Boltzmann transport theory. Within this framework the thermopower is governed by the energy derivative of the conductivity, strongly favoring heavy band mass materials (note that ZT is proportional to the square of S), while the conductivity has an opposite but weaker dependence on the band mass. In fact, Mahan and Sofo argued that the ideal band structure for a thermoelectric material consists of an infinitely heavy, i.e., dispersionless, band with a delta function density of states.[5] One way of obtaining such a band structure is to consider a material consisting of clusters that contribute to the active band and then increasing the spacing between the clusters to reduce the hopping and consequently the band width. The problem is that it will be increasingly difficult to stay within the regime of Boltzmann transport as the band mass increases since the electronic structure will be increasingly prone to localization both due to disorder (Anderson localization) and Coulomb repulsion (Mott localization). Such localization generally is expected to result in a strong suppression of the conductivity and therefore ZT.

The dilemma posed by the conflicting preferences on the carrier effective mass by high thermopower and high carrier mobility may be circumvented by using materials with both heavy and light bands near the Fermi level, such as filled *p*-type skutterudites[6] and lanthanum telluride.[7] This may also be achieved by introducing impurities that induce impurity bands with little dispersion near the edge of a dispersive valance or conduction band.[8] These provide ways of avoiding localization while still having very heavy bands involved in the transport.

As mentioned, low thermal conductivity is also important for high ZT. The lattice thermal conductivity can be reduced by increasing phonon scattering through several strategies, e.g., alloying to introduce large atomic mass difference, nanostructuring,[9,10] focusing on materials with complex crystal structures, and materials that have loosely bound (rattling) ions,[11,12] or more generally anharmonic coupling between acoustic and low frequency optical branches.[13]

Complex Zintl-phase materials appear to be promising candidates for thermoelectric applications.[14] In general, the Zintl-phase compounds are valence precise semiconductors with electropositive cations and covalently bonded anionic units or networks formed from more electronegative elements. These often have small band gaps and benefit from the flexibility of alloying on the cation sites to obtain doping

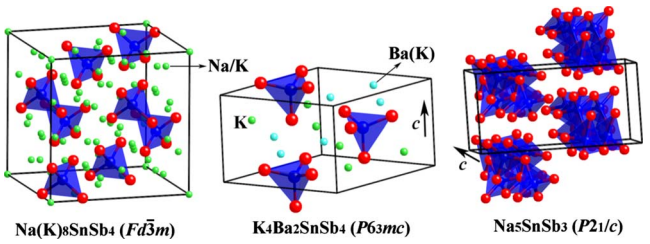

FIG. 1. (Color online) Crystal structures of Zintl-phase compounds containing $SnSb_4$ tetrahedra: (a) $Na(K)_8SnSb_4$, (b) $K_4Ba_2SnSb_4$, (c) Na_5SnSb_3. The Sn atoms (blue spheres) sit at the centers of the tetrahedra formed by Sb atoms (red spheres). The interstitial Na, K and Ba cations in (a) and (b) are all depicted as smaller light spheres. For Na_5SnSb_3, the Na cations are not shown for clarity and the $SnSb_4$ tetrahedra are vertex shared to form chain-like structures. The unit cells are shown using black lines and in (a) the crystal lattice is shifted by (0.125,0.125,0.125) with respect to the standard setting in order to include all the $SnSb_4$ tetrahedra in the cell.

without strongly perturbing the anionic network that often plays the main role in the electrical transport. In addition, the heavy atoms, complex structures, and soft lattices of many of these materials may lead to low lattice thermal conductivity. Recently, many Zintl-phase compounds, especially antimonides, with good thermoelectric performance have been reported. These include Zn_4Sb_3, $Yb_{14}MnSb_{11}$, $Ca_xYb_{1-x}Zn_2Sb_2$, $YbCd_{2-x}Zn_xSb_2$, and filled skutterudites.[12,15–18]

Previous thermoelectric studies on the Zintl-phase compounds have been largely focused on the crystals with covalently bonded polyanion networks that provide high mobility for carrier transport.[14] These materials can exploit the flexibility of Zintl chemistry by using the cation site both for doping and alloying (leading to reduction in the thermal conductivity, as e.g., in skutterudites with alloying on the filling site[19]).

Here we explore another type of Zintl compound for their potential thermoelectric applications. These compounds have weakly coupled anionic clusters and intercalated cations. The cohesion of these crystals is provided mainly by the ionic bonding between the cations and the anionic clusters.

We investigated the electronic structure and phonon properties of several Zintl-phase compounds with above-mentioned structural properties. We show that $Na(K)_8SnSb_4$ and related materials[20–22] may be good thermoelectric materials. The basic structural feature of these compounds is the composition of weakly coupled $SnSb_4$ tetrahedra and intercalated alkali or alkaline earth cations as shown in Fig. 1(a) for the example of Na_8SnSb_4. Although these materials were synthesized in the 1980s, there has been little characterization of their physical properties, presumably because of their chemically reactive nature. In any case, the weakly coupled anionic clusters may be expected to have weakly overlapping cluster electronic states that form heavy valence bands with very small dispersion. However, we find that in addition, there are more dispersive bands near the valence band edge. Therefore these materials have a combination of very narrow bands and more dispersive bands near the valence band edge, which is a highly favorable situation for thermoelectric performance. We find that the occurrence of this type of band structure can be understood on simple chemical terms and is expected quite generally in this type of compound and furthermore the weak bonding of these materials leads to soft lattices that may be expected to have low thermal conductivity. As such, this may provide an avenue for finding useful thermoelectric materials.

II. METHODOLOGY

Electronic structure calculations were performed within the local density approximation (LDA), using the general potential linearized augmented plane-wave (LAPW) method with local orbitals as implemented in the WIEN2K code.[23–25] Core states were treated fully relativistically while for valence states the spin-orbit interaction was included using the second variational method. This is potentially important because of the involvement of Sn and Sb p states in the electronic structure. LAPW spheres of radius $2.0a_0$ for Na, $2.1a_0$ for K, $2.4a_0$ for Ba, and $2.3a_0$ for Sn and Sb were used. We employed well-converged basis sets determined by $R_{\min}k_{\max}=8.0$, where $R_{\min}$ is the minimum LAPW sphere radius and $k_{\max}$ is the plane-wave cutoff for the interstitial region. Local orbitals were included to accurately treat semicore states. For all compounds, the experimental lattice constants were used and the internal atomic coordinates were optimized by total-energy minimization.

We performed thermopower calculations starting from our first principles band structures, as well as phonon calculations for $Na(K)_8SnSb_4$. The thermopower was calculated based on Boltzmann transport theory with the constant scattering time approximation, as implemented in the BoltzTraP program.[26] Very dense k-meshes [up to 80 000 points in the full Brillouin zone (BZ)] were used for these calculations. The lattice dynamics calculations were performed using the frozen phonon method,[27,28] as implemented in the FROPHO code.[29] The required forces on atoms to evaluate the force constants were calculated using the projector augmented wave (PAW) method as implemented in the VASP code.[30,31] The kinetic energy cutoff for the plane-wave basis sets used in the PAW-LDA calculations was chosen to be 260 eV. The PAW calculations yielded results for relaxed crystal structures and electronic structures that are nearly identical to those obtained from the LAPW method.

III. STRUCTURE

As shown in Fig. 1(a), Na_8SnSb_4 and K_8SnSb_4 crystallize in the face-centered cubic structure (space group $Fd\bar{3}m$).[20,21] Sn occupies the $8a$ (0,0,0) sites, tetrahedrally coordinated by the Sb atoms at the $32e$ sites (x_{Sb},x_{Sb},x_{Sb}) forming $SnSb_4$ tetrahedra. Viewed from the center of a tetrahedron, each vertex points along a [111] direction. The intercalated Na/K cations are located at the sites $16c$ (0.125,0.125,0.125) and $48f$ $(x_c,0,0)$. As mentioned, the experimental lattice parameters of $a=14.816$ Å for Na_8SnSb_4 and 16.279 Å for K_8SnSb_4 were used and the internal atomic coordinates were fully optimized. For Na_8SnSb_4, the optimized values of x_{Sb}

and x_c are 0.3605 and 0.2703, in good agreement with the experimental values of 0.3608 and 0.2728. The Sn-Sb bond length is 2.8 Å within a tetrahedron, and the distance between any two Sb atoms in the same tetrahedron is 4.6 Å. The shortest distance between the two Sb atoms from different adjacent tetrahedra is significantly longer at 5.3 Å.

The structure of $K_4Ba_2SnSb_4$ [Fig. 1(b)] is related to that of Na_8SnSb_4. Both may be described as consisting of $SnSb_4$ tetrahedra and intercalated cations. However, the $SnSb_4$ tetrahedra are located at the hexagonal-close-packed sites in $K_4Ba_2SnSb_4$, leading to a hexagonal $P6_3mc$ structure.[22] One of the threefold axes for any tetrahedron is aligned along the [0001] hexagonal direction. The K cations are located at two inequivalent interstitial sites and Ba atoms partially substitute one of the two K sites. We use the virtual crystal approximation to simulate the partial Ba substitution. This is justified by the fact that the electronic states of these electropositive elements are high in the conduction bands (see below) in these Zintl type compounds. Also, the optimized internal coordinates show good agreement with experimental values, indicating the validity of this approach. The shortest distance between the two Sb atoms from two adjacent tetrahedra is nearly same as that in Na_8SnSb_4, ~5.3 Å.

Finally, we consider one compound with connected tetrahedra. Figure 1(c) shows the structure of Na_5SnSb_3 (space group $P2_1/c$).[21] The $SnSb_4$ tetrahedra are connected by sharing one Sb atom at the vertex. This forms the quasi-one-dimensional spiral chainlike structures arranged along the c-axis direction. For clarity, the intercalated Na ions in the interstitial sites are not shown in Fig. 1(c).

IV. ELECTRONIC STRUCTURE

The calculated band structure and electronic density of states (DOS) for Na_8SnSb_4 and K_8SnSb_4 are shown in Figs. 2 and 3, respectively. As seen, both compounds are narrow-gap semiconductors and have similar electronic structures. The conduction band minimum (CBM) and the valence band maximum (VBM) are both slightly off the Γ point, resulting in indirect band gaps of 0.08 and 0.15 eV within the LDA for Na_8SnSb_4 and K_8SnSb_4, respectively. However, because of the very flat top valence band the energy difference between the true valence band maximum and the maximum at Γ is very small, and therefore this is effectively a direct gap. We emphasize that these are density functional calculations and as such that the band gaps may be underestimated. It will be of interest to compare with spectroscopic data if such data becomes available.

Figure 3 shows that the Sn-p states are mainly concentrated at higher binding energy and strongly hybridize with the Sb-p states forming covalent Sn-Sb bonds within the $SnSb_4$ tetrahedra. The edges of both the valence and conduction bands are dominated by Sb-p states. The Na/K derived bands are found at high energies in the conduction bands, and therefore these alkali metal atoms are essentially fully ionic, consistent with the usual bonding picture for Zintl compounds.

The dominant Sb-p states near the VBM mostly originate from the electron lone pairs on the Sb. The Sb lone pair

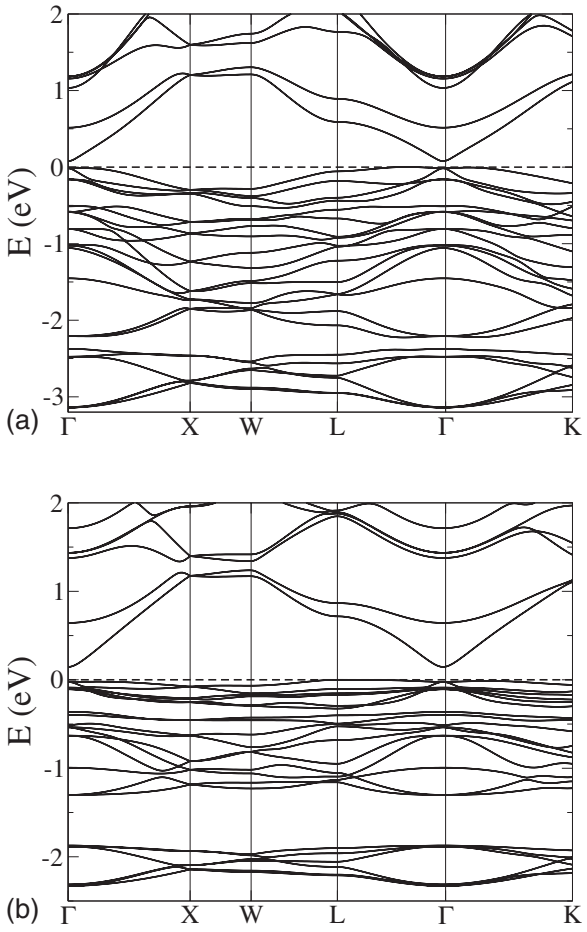

FIG. 2. Electronic band structures of (a) Na_8SnSb_4 and (b) K_8SnSb_4. The valence band edge is set as energy zero and denoted with a dashed line.

derived states form heavy bands with small dispersion. At the edge of the valence bands, we find heavy bands for both Na_8SnSb_4 and K_8SnSb_4. The resulting high DOS near the VBM should lead to large thermopower in p-type materials. This narrow band arises from the Sb states localized within $SnSb_4$ clusters as shown in Fig. 4(a) for Na_8SnSb_4. The weak intercluster coupling causes some dispersion for the Sb bands near the VBM.

The Sb states associated with the shortest intercluster Sb-Sb distance should have the strongest coupling and thus form the most dispersive band. This band should be close to the VBM since the relatively extensive Sb states that form the band should have low binding energies (in other words they are weakly bonding or nonbonding within the cluster) and their stronger coupling results in larger level repulsion that pushes the antibonding state to higher energy. Indeed, we find a light band near the VBM that is as dispersive as the lowest conduction band and is nearly degenerate with the heavy band near the Γ point. The presence of this light band, which can be easily accessed for hole transport, is extremely important as it may be expected to promote carrier conductivity that is essential in thermoelectric materials. The dispersion of the light band in Na_8SnSb_4 has a Kane band shape with a near linear dispersion away from the band edge and a closely matching conduction band. Figure 4(b) shows the

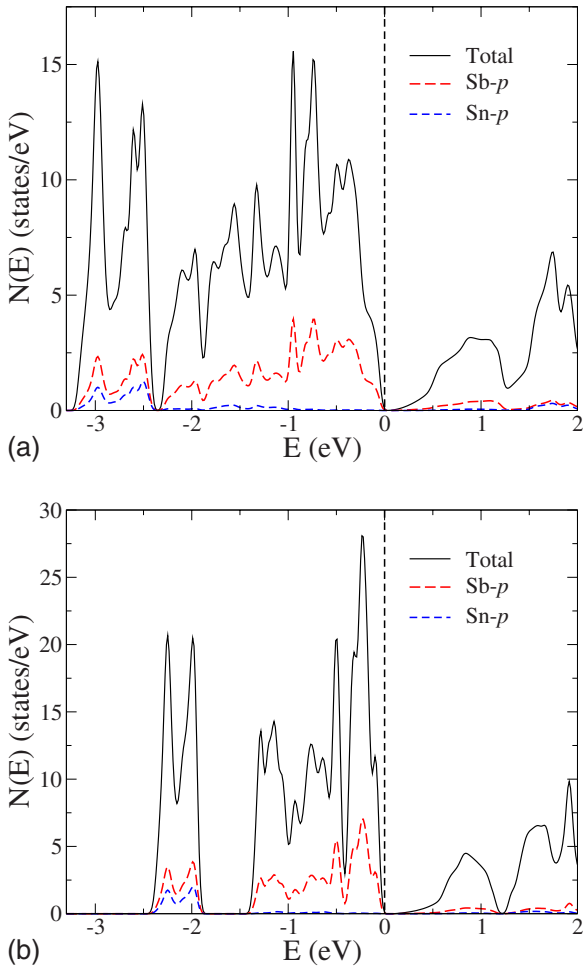

FIG. 3. (Color online) Calculated total and projected DOS for (a) Na_8SnSb_4 and (b) K_8SnSb_4. Since the projections are onto LAPW spheres, the Sb-*p* DOS are significantly underestimated owing to the more extended Sb orbitals and only the scale is proportional to the real value. All the values are in per formula unit.

charge density contours for the dispersive valence band near the VBM. This clearly shows the significant charge overlap between the two Sb atoms from the adjacent $SnSb_4$ clusters. Such charge overlap exists despite the relatively large Sb-Sb separation of 5.3 Å, as compared to the normal Sb-Sb covalent bond length of 2.8 Å. It appears therefore that the Sb-*p* states are quite spatially extended. This may be a consequence of the attractive potential provided by the interstitial cations and importantly the very high charge state of the $(SnSb_4)^{8-}$ clusters. This spatial extension leads to a connection between these anions for transport in the dispersive band.

The narrower valence bands of K_8SnSb_4 as compared to Na_8SnSb_4 reflect the somewhat larger separation between $SnSb_4$ clusters in K_8SnSb_4 and hence reduced intercluster interactions. We find that replacing Na or K by a smaller Li atom while leaving the lattice parameters unchanged has a negligible effect on the light band. This further demonstrates that the direct Sb-Sb coupling is responsible for the intercluster interaction. The combination of heavy and light bands is favorable for the thermoelectric materials since it provides

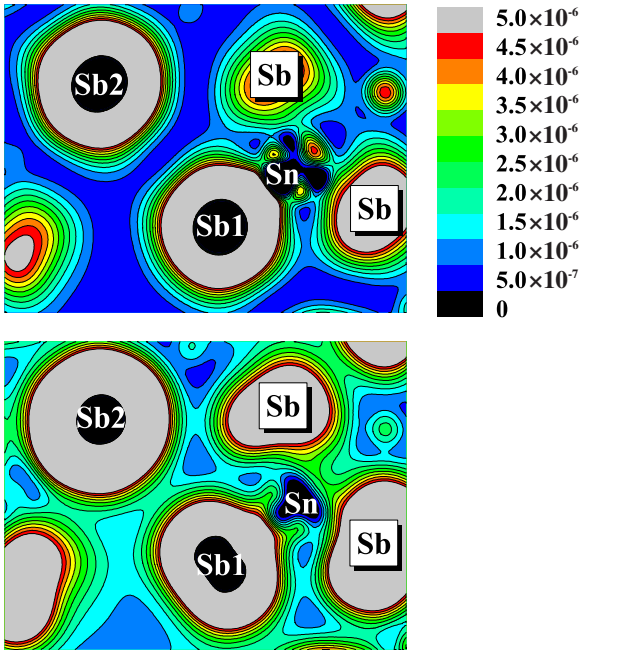

FIG. 4. (Color online) Charge density contours for the states of the heavy (upper panel) and light (lower panel) bands near the VBM (along $\Gamma-L$ direction) for Na_8SnSb_4. The contours are in a plane determined by three points: one Sn atom and one of the four antimony atoms (Sb1) within a tetrahedron, and another antimony atom (Sb2) in an adjacent tetrahedron.

both high thermopower and reasonably good carrier mobility, as in filled skutterudites and La-Te.[6,7]

The favorable band features near the VBM, as discussed above, suggest that good thermoelectric performance may be possible with *p*-type doping. Considering the chemistry of these materials, one likely avenue for this is the introduction of vacancies on the alkali metal lattice. We studied the hole-doping dependence (up to 0.2 holes/f.u.) of the electronic structure for Na_8SnSb_4. This was done using the virtual crystal approximation. Specifically, we reduced the nuclear charges on the Na sites. The resulting electronic structure was quite similar to the original band structure with a downshift of the Fermi level, consistent with rigid-band behavior. This rigid-band behavior in virtual crystal calculations is generally a sign of weak scattering, which also might be expected based on the very weak contribution of the cations to the electronic structure near the band edges and the spatial separation of this doping site from the anionic clusters that do form the bands. In other words, the acceptor-induced hole scattering for this type of doping is expected to be weak since the hole conduction is in the anion network, which is not covalently bonded with cations.

V. THERMOPOWER

We performed calculations of the thermopower as a function of temperature within constant scattering time approximation Boltzmann theory in order to quantify the effects of the mixed heavy/light valence band structure on the transport. Within this approach the temperature and doping level

dependent thermopower, $S(T,\mu)$ is obtained from the following:[32,33]

$$S_{\alpha\beta} = \sum_{\gamma} (\sigma^{-1})_{\alpha\gamma} \nu_{\beta\gamma}, \tag{1}$$

where σ is the electronic conductivity given by

$$\sigma_{\alpha\beta}(T,\mu) = \frac{1}{\Omega} \int \sigma_{\alpha\beta}(\varepsilon) \left[-\frac{\partial f_{\mu}(T,\varepsilon)}{\partial \varepsilon} \right] d\varepsilon, \tag{2}$$

and

$$\nu_{\alpha\beta}(T,\mu) = \frac{1}{eT\Omega} \int \sigma_{\alpha\beta}(\varepsilon)(\varepsilon - \mu) \left[-\frac{\partial f_{\mu}(T,\varepsilon)}{\partial \varepsilon} \right] d\varepsilon. \tag{3}$$

Here the $\varepsilon_{i,\mathbf{k}}$ are electron band energies, f_{μ} is the Fermi distribution function, μ is the chemical potential (which is T dependent), T is temperature and Ω is volume. The essential ingredient, the energy projected conductivity tensors (transport distributions) are

$$\sigma_{\alpha\beta}(\varepsilon) = \frac{1}{N} \sum_{i,\mathbf{k}} \sigma_{\alpha\beta}(i,\mathbf{k}) \delta(\varepsilon - \varepsilon_{i,\mathbf{k}}), \tag{4}$$

and can be obtained using **k**-dependent conductivity tensor

$$\sigma_{\alpha\beta}(i,\mathbf{k}) = e^2 \tau_{i,\mathbf{k}} v_{\alpha}(i,\mathbf{k}) v_{\beta}(i,\mathbf{k}), \tag{5}$$

where N represents the number of k point sampled in the BZ, $\tau_{i,\mathbf{k}}$ is scattering time and $v_{\alpha}(i,\mathbf{k})$ is the component of band velocity that can be straightforwardly obtained from the band structure.

We note that in all the above expressions only the scattering time τ cannot be evaluated from the band structure. Fortunately, in most degenerately doped semiconductors and metals, τ is usually a weak function of energy on the scale of KT and can be approximately treated as a constant. This is the so-called constant scattering time approximation (CSTA), which neglects the weak energy dependence of τ but retains the possibly strong temperature and doping dependence.[34,35] Within the CSTA, τ is exactly canceled in the expression of thermopower [Eq. (1)]. Thus with this approximation, the thermopower can be directly evaluated from the first principles band structures. As mentioned, we used the BoltzTraP program for this purpose.[26]

The essential point is that for at the given doping level and temperature the scattering time is assumed to be the same for all carriers independent of their energy. This also implies that carriers in different bands are assumed to have the same scattering rate. This is clearly suspect in cases where bands have very different character, for example in materials with f bands and valence bands, and also in cases with strongly energy dependent scattering mechanisms, such as due to Kondo physics. Nonetheless, it appears to hold remarkably well in a wide variety of metals and thermoelectric materials. The Boltzmann kinetic transport theory within the CSTA has been successfully applied to many thermoelectric materials including degenerately doped semiconductors, Zintl type phases and oxides.[26,36–43] Agreement with experiment has been obtained diverse materials such as skutterudites,[44,45] the high temperature chalcogenide material, La-Te.[7] and even the oxide thermoelectric, Na_xCoO_2, which is near magnetism and perhaps quantum criticality associated with this.[42,43,46–48] Finally, we note that we rely on the band structures calculated at zero temperature in order to perform the transport calculations. Although in general, the electronic structure can be temperature dependent. The effect of the temperature dependence of the band structure is presumably a minor effect on the transport coefficients, the main effects being the temperature dependent scattering rates and the broadening of the Fermi distribution with temperature.

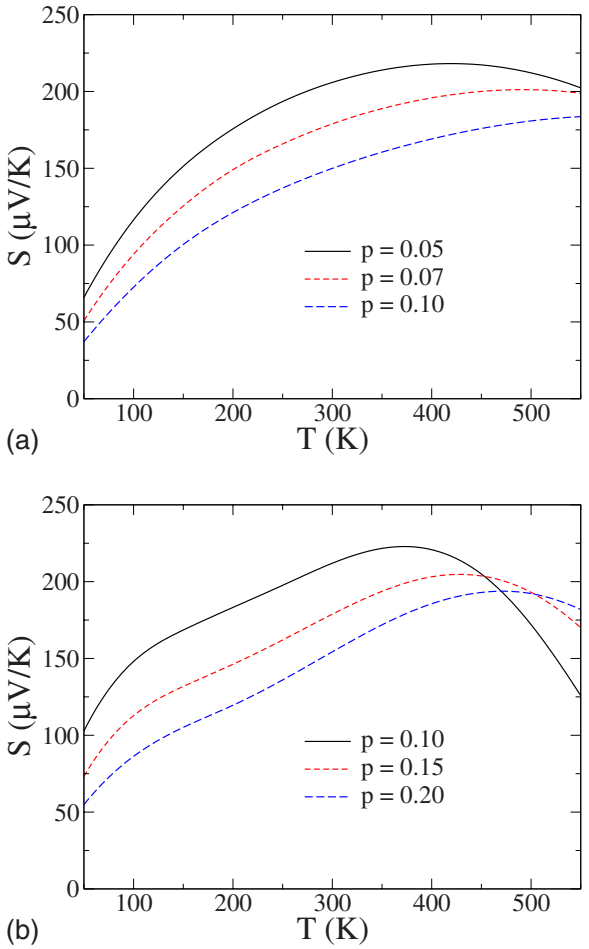

FIG. 5. (Color online) Calculated Seebeck coefficient as a function of temperature for p-type (a) Na_8SnSb_4 and (b) K_8SnSb_4. The doping levels are given in holes per $Na(K)_8SnSb_4$ unit.

We calculated the thermopower for hole-doped $Na(K)_8SnSb_4$, as a function of temperature and doping level. As mentioned, the electronic structure of the hole-doped $Na(K)_8SnSb_4$ shows the rigid-band behavior. Thus the thermopower was calculated using the undoped band structure with appropriate temperature dependent shifts of the Fermi level to correspond to the doping level.

The low melting temperature of $Na(K)_8SnSb_4$ means that at best it can be used as a low-temperature thermoelectric material. Figure 5 shows the calculated isotropic thermopower $S(T)$ for cubic $Na(K)_8SnSb_4$ as a function of temperature (up to 550 K) at selected p-type doping levels. One can see that the heavy band at the edge of valence bands indeed leads to a high thermopower in the temperature range for cooling applications. In particular, a large value of ther-

mopower above 160 μV/K can be maintained in the temperature range of 350–550 K with doping levels as high as 0.1 holes/f.u. The multiband nature of the transport may be seen in the shape of $S(T)$, which is enhanced at low T. For K_8SnSb_4, the heavier valence band results in higher thermopower and the doping level that maintains the thermopower above 160 μV/K is increased to 0.2 holes/f.u. At 0.1 holes/f.u., the high thermopower spans the temperature range of 200–500 K. The decline of the thermopower at high temperatures (especially for low doping levels) is caused by thermally activated minority carriers.

VI. PHONONS

For a good thermoelectric material, the thermal conductivity, especially the lattice part κ_l, must be low. Materials with soft lattices, specifically low sound velocities, have intrinsically lower thermal conductivities than those with high sound velocities. Furthermore, strong scattering of the heat-carrying acoustic phonons is desirable. This can be realized in materials with loosely bonded structural components. In particular, this favors low velocity acoustic phonons, as well as low lying optical phonon branches that induce scattering due to their anharmonic coupling to the acoustic modes. For example, some materials have large internal voids that can be filled by so-called rattling ions. These weakly bonded rattling ions have low vibrational frequencies and can be effective in scattering the acoustic phonons.[11,12] $Na(K)_8SnSb_4$ consists of weakly coupled clusters, which are likewise expected to produce soft phonons. Indeed, the calculated phonon dispersions for $Na(K)_8SnSb_4$ (see Fig. 6) show that some optical modes have very low frequencies of less than $\sim$50 cm^{-1} and are mixed with the acoustic modes. These optical modes originate from Sb vibrations within the $SnSb_4$ clusters. For comparison, the frequencies of these optical modes are even lower than the calculated frequency ($\sim$60 cm^{-1}) for the vibrations of the La ions in filled skutterudites, $La(Fe,Co)_4Sb_{12}$.[13] This suggests effective coupling between these soft optical phonons and the acoustic phonons, leading to enhanced scattering and hence lower κ_l. In fact, the very soft lattice of this anionic cluster compound and low optic phonon frequencies imply that the thermal conductivity may be very low.

VII. $K_4Ba_2SnSb_4$ AND Na_5SnSb_3

As mentioned, p-type $Na(K)_8SnSb_4$ may show good thermoelectric performance. However, the high content of alkali elements in these compounds is expected to cause chemical instability of the materials in air. For this reason, we have also considered some other Zintl-phase compounds with lower content of alkali elements.

Substituting alkali elements with alkaline earth elements may be an effective way of improving the chemical stability of the materials. $K_4Ba_2SnSb_4$ (Ref. 22) is a known compound with partial substitution of K by Ba. It would be desirable to investigate whether $(SnSb_4)^{8-}$ compounds with still lower alkali contents or even no alkali elements can be synthesized. The calculated band structure for $K_4Ba_2SnSb_4$ (see

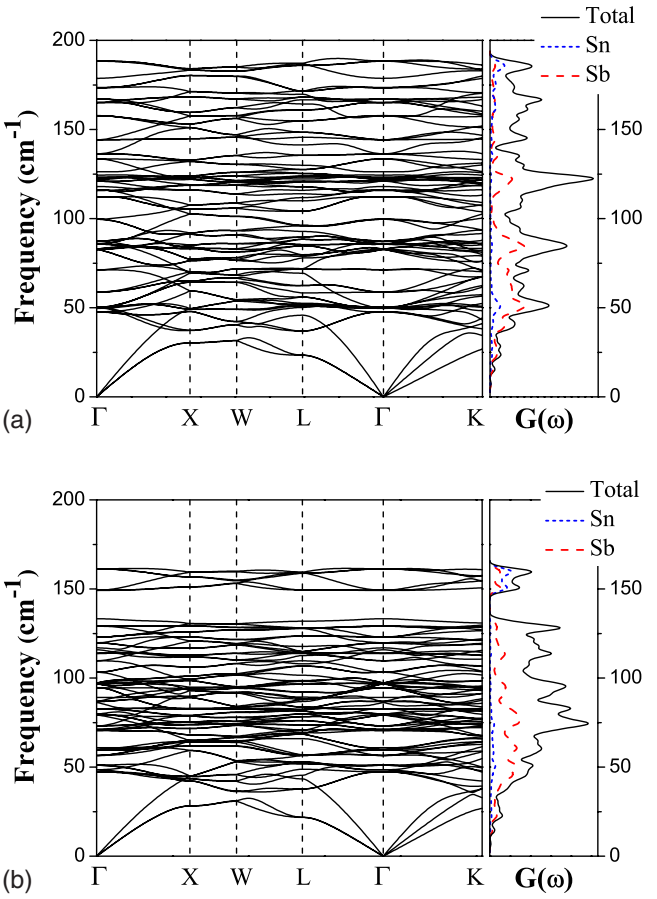

FIG. 6. (Color online) Calculated phonon dispersion curves and density of states for (a) Na_8SnSb_4 and (b) K_8SnSb_4. The phonon DOS projected onto Sn and Sb atoms are also shown.

Fig. 7) shows that it is a semiconductor with a direct band gap of 0.16 eV within LDA. $K_4Ba_2SnSb_4$ and K_8SnSb_4 have the same network of $SnSb_4$ clusters and the resulting band structures are also similar in terms of the lower-lying Sn-Sb bonding states and the higher-lying Sb-dominated states near the band gap. The heavy and light bands of $K_4Ba_2SnSb_4$ are split, as can be seen in Fig. 7. The stronger coupling of the $SnSb_4$ clusters along the c axis (with the shortest intercluster Sb-Sb distance) leads to larger dispersion of the light band along the Γ-A (the c axis) direction. This further confirms that the large dispersion of the light band near the VBM arises from the intercluster Sb state overlap.

Na_5SnSb_3 is also a narrow-gap semiconductor with a band gap of 0.07 eV within LDA. It also has an anisotropic crystal structure with Sb-vertex-shared $SnSb_4$ clusters along the c-axis forming chainlike structures. As a result, the dispersion of the valence band edge states is larger in the Γ-Z direction, suggesting higher hole mobility along the c axis although the anisotropy is lower than in $K_4Ba_2SnSb_4$. The heavy and light bands near the VBM are split in Na_5SnSb_3. The light band has higher binding energy but may be accessible for hole transport with heavy p-type doping.

VIII. SUMMARY AND CONCLUSIONS

We used first principles methods to study the electronic structure, transport properties and phonon spectra of the

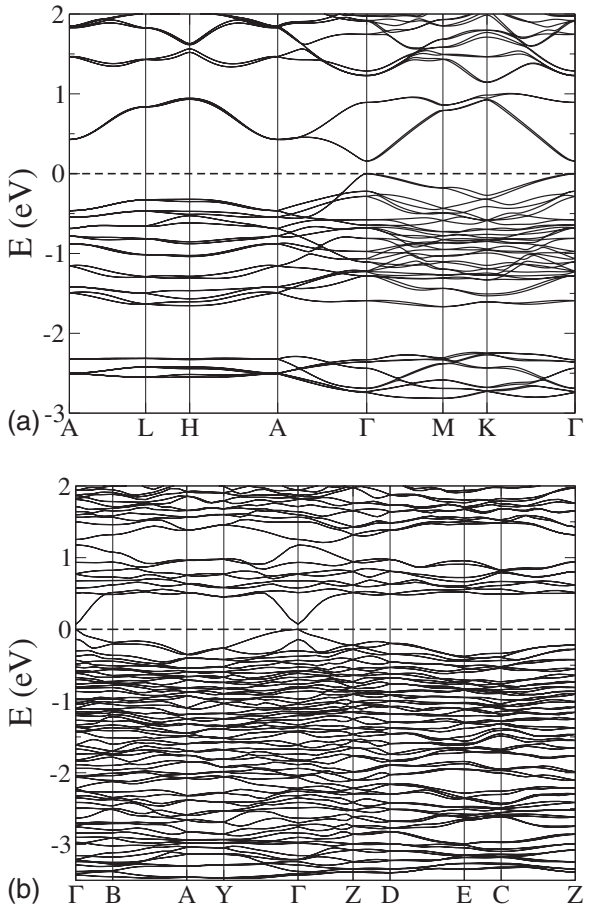

FIG. 7. Calculated band structure of (a) hexagonal $K_4Ba_2SnSb_4$ and (b) monoclinic Na_5SnSb_3. For Na_5SnSb_3 the dense bands result from the large unit cell that contains 72 atoms.

Zintl-phase compounds, Na_8SnSb_4 and K_8SnSb_4. The results indicate that these may be good *p*-type thermoelectric materials for the following reasons: (1) they have a combination of heavy and light bands near the VBM, allowing high thermopower and reasonably good hole conductivity; (2) the needed *p*-type doping can very likely be achieved by introducing Na or K vacancies, which are not expected to cause strong hole scattering since they are not covalently bonded with the network of the anionic clusters in which the hole transport occurs; (3) the weakly coupled cluster structures should lead to low thermal conductivity. The calculated low-frequency intracluster optical phonons are expected to effectively scatter the heat-carrying acoustic phonons, further reducing the thermal conductivity; (4) they are isotropic, good for material growth and device construction.

The existence of both heavy and light bands near the VBM is also due to the structural features of these compounds. The localized intracluster states gives rise to the heavy bands, while the weak intercluster interaction leads to the light band. Sb is effective in forming an anion network for hole transport as its extended *p* states especially in these highly charged anionic clusters dominate the intercluster coupling.

However, Na_8SnSb_4 and K_8SnSb_4 have low melting temperatures and thus could only be suitable for low-temperature thermoelectric applications. Furthermore, the high alkali element contents in these compounds very likely cause chemical instability in air. This motivated us to study several other Zintl-phase compounds with $SnSb_4$ anion networks but lower alkali contents, i.e., $K_4Ba_2SnSb_4$ and Na_5SnSb_3. These compounds have split heavy and light bands near the VBM.

The structural feature of weakly coupled anionic clusters is the key to the good thermoelectric properties of the materials studied here. Such clusters will generally have an electronic structure governed by internal bonding, with band formation due to the intercluster interaction in the solid. Considering only a single ionic cluster, the highest occupied states are expected to be those with the least favorable bonding configurations, while the lowest energy states will be those that correspond to stronger bonding. The weakly bonding (and therefore highest energy) occupied states will therefore naturally be states with orbital character that is stronger pointing out of the cluster as compared to the lower energy states, which will be more directly connected with the cohesion of the clusters. Therefore some of these states, specifically those directed at adjacent clusters, will also be more dispersive than the more strongly bonding valence states. As such, one may generally expect that there will be more dispersive bands at or near the top of the valence band. In fact, our calculations show a combination of heavy and light bands near the valence band maxima for all the compounds studied, and based on this and the above discussion, we expect that while the exact placement and dispersion of the bands will depend on details, this presence of heavy and light bands near the valence band maximum may be rather common in Zintl compounds composed of anionic clusters.

Many other materials with similar structural properties remain to be explored for their potential thermoelectric applications. The approaches used in the present study may also be useful for guiding future search of new high-performance thermoelectric materials.

ACKNOWLEDGMENTS

This work was supported by the U.S. Department of Energy, Assistant Secretary for Energy Efficiency and Renewable Energy, Office of Vehicle Technologies, Propulsion Materials Program (M.H.D., D.J.S.) and the S3TEC Energy Frontier Research Center (D.J.S.) and the Office of Basic Energy Sciences, Division of Materials Sciences and Engineering (L.Z., D.J.S.).

[1] T. M. Tritt and M. A. Subramanian, MRS Bull. **31**, 188 (2006).
[2] G. J. Snyder and E. S. Toberer, Nature Mater. **7**, 105 (2008).
[3] G. S. Nolas, J. Poon, and M. Kanatzidis, MRS Bull. **31**, 199 (2006).
[4] To a good approximation of elastic scattering, the electrical thermal conductivity (κ_e) could be connected to the electrical conductivity (σ) through the Wiedemann-Franz relationship, $\kappa_e = L_0 \sigma T$, which leads to $ZT = (S^2/L_0)/(1+\kappa_l/\kappa_e)$. This means, to reach the state-of-art value of $ZT=1$, the minimum thermopower, S_m is 157 μV/K, with the Lorenz factor for free electrons, 2.45×10^{-8} V^2/K^2.
[5] G. D. Mahan and J. O. Sofo, Proc. Natl. Acad. Sci. U.S.A. **93**, 7436 (1996).
[6] D. J. Singh and I. I. Mazin, Phys. Rev. B **56**, R1650 (1997).
[7] A. F. May, D. J. Singh, and G. J. Snyder, Phys. Rev. B **79**, 153101 (2009).
[8] J. P. Heremans, V. Jovovic, E. S. Toberer, A. Saramat, K. Kurosaki, A. Charoenphakdee, S. Yamanaka, and G. J. Snyder, Science **321**, 554 (2008).
[9] B. Poudel, Q. Hao, Y. Ma, Y. Lan, A. Minnich, B. Yu, X. Yan, D. Wang, A. Muto, D. Vashaee, X. Chen, J. Liu, M. S. Dresselhaus, G. Chen, and Z. Ren, Science **320**, 634 (2008).
[10] T. C. Harman, P. J. Taylor, M. P. Walsh, and B. E. LaForge, Science **297**, 2229 (2002).
[11] G. A. Slack, in *CRC Handbook of Thermoelectrics*, edited by M. Rowe (CRC, Boca Raton, Florida, 1995), pp. 407–440.
[12] B. C. Sales, D. Mandrus, and R. K. Williams, Science **272**, 1325 (1996).
[13] J. L. Feldman, D. J. Singh, C. Kendziora, D. Mandrus, and B. C. Sales, Phys. Rev. B **68**, 094301 (2003).
[14] S. M. Kauzlarich, S. R. Brown, and G. J. Snyder, Dalton Trans. **2007**, 2099 (2007).
[15] T. Caillat, J. P. Fleurial, and A. Borshchevsky, J. Phys. Chem. Solids **58**, 1119 (1997).
[16] G. J. Snyder, M. Christensen, E. Nishibori, T. Caillat, and B. B. Iversen, Nat. Mater. **3**, 458 (2004).
[17] S. R. Brown, S. M. Kauzlarich, F. Gascoin, and G. J. Snyder, Chem. Mater. **18**, 1873 (2006).
[18] F. Gascoin, S. Ottensmann, D. Stark, S. M. Haile, and G. J. Snyder, Adv. Funct. Mater. **15**, 1860 (2005).
[19] J. Yang, G. P. Meisner, C. J. Rawn, H. Wang, B. C. Chakoumakos, J. Martin, G. S. Nolas, B. L. Pedersen, and J. K. Stalick, J. Appl. Phys. **102**, 083702 (2007).
[20] B. Eisenmann, J. Klein, and J. Z. Naturforsch, B: Chem. Sci. **43**, 69 (1988).
[21] B. Eisenmann, J. Klein, and J. Z. Naturforsch, B: Chem. Sci. **43**, 1156 (1988).
[22] B. Eisenmann and U. Rossler, Z. Anorg. Allg. Chem. **626**, 1373 (2000).
[23] E. Sjöstedt, L. Nordström, and D. J. Singh, Solid State Commun. **114**, 15 (2000).
[24] D. J. Singh and L. Nordstrom, *Planewaves, Pseudopotentials, and the LAPW Method*, 2nd ed. (Springer, Berlin, 2006).
[25] P. Blaha, K. Schwarz, G. Madsen, D. Kvasnicka, and J. Luitz, *WIEN2k, An Augmented PlaneWave+Local* Orbitals Program for Calculating Crystal Properties (K. Schwarz, Tech. Univ., Wien, Austria, 2001).
[26] G. K. H. Madsen and D. J. Singh, Comput. Phys. Commun. **175**, 67 (2006).
[27] D. Alfè, G. D. Price, and M. J. Gillan, Phys. Rev. B **64**, 045123 (2001).
[28] K. Parlinski, Z-. Q. Li, and Y. Kawazoe, Phys. Rev. Lett. **78**, 4063 (1997).
[29] A. Togo, F. Oba, and I. Tanaka, Phys. Rev. B **78**, 134106 (2008).
[30] G. Kresse and D. Joubert, Phys. Rev. B **59**, 1758 (1999).
[31] G. Kresse and J. Furthmüller, Phys. Rev. B **54**, 11169 (1996).
[32] J. M. Ziman, *Principles of the Theory of Solids* (Cambridge University Press, Cambridge, 1979).
[33] P. B. Allen, W. E. Pickett, and H. Krakauer, Phys. Rev. B **37**, 7482 (1988).
[34] W. Jones and N. H. March, *Theoretical Solid State Physics* (Courier Dover Publications, New York, 1985).
[35] J. B. Smith and H. Ehrenreich, Phys. Rev. B **25**, 923 (1982).
[36] D. J. Singh, *Semiconductors and Semimetals* (Academic, New York, 2000), Vol. 70: Thermoelectric Materials Research.
[37] G. K. H. Madsen, K. Schwarz, P. Blaha, and D. J. Singh, Phys. Rev. B **68**, 125212 (2003).
[38] L. Bertini and C. Gatti, J. Chem. Phys. **121**, 8983 (2004).
[39] L. Lykke, B. B. Iversen, and G. K. H. Madsen, Phys. Rev. B **73**, 195121 (2006).
[40] L. Zhang and D. J. Singh, Phys. Rev. B **80**, 075117 (2009).
[41] Y. Wang, X. Chen, T. Cui, Y. Niu, Y. Wang, M. Wang, Y. Ma, and G. Zou, Phys. Rev. B **76**, 155127 (2007).
[42] D. J. Singh and D. Kasinathan, J. Electron. Mater. **36**, 736 (2007).
[43] H. J. Xiang and D. J. Singh, Phys. Rev. B **76**, 195111 (2007).
[44] D. J. Singh and W. E. Pickett, Phys. Rev. B **50**, 11235 (1994).
[45] D. T. Morelli, T. Caillat, J. P. Fleurial, A. Borshchevsky, J. Vandersande, B. Chen, and C. Uher, Phys. Rev. B **51**, 9622 (1995).
[46] I. Terasaki, Y. Sasago, and K. Uchinokura, Phys. Rev. B **56**, R12685 (1997).
[47] D. J. Singh, Phys. Rev. B **61**, 13397 (2000).
[48] D. J. Singh, Phys. Rev. B **68**, 020503(R) (2003).